Received: 12 May 2018 | Revised: 17 March 2019 | Accepted: 9 April 2019

DOI: 10.1111/sum.12519

RESEARCH PAPER

Soil Use and Management | BRITISH SOCIETY OF SOIL SCIENCE | WILEY

Evaluation of rainfall kinetic energy and erosivity in northern Taiwan using kriging with climate characteristics

Kuo-Wei Liao[1] | **Jia-Jun Guo**[1] | **Jen-Chen Fan**[1] | **Cheng-Chun Lee**[2] | **Chien Lin Huang**[3]

[1]Department of Bioenvironmental Systems Engineering, National Taiwan University, Taipei, Taiwan

[2]Soil and Water Conservation Bureau, Council of Agriculture, Executive Yuan, Taipei, Taiwan

[3]hetengtech Company Limited, Taipei, Taiwan

Correspondence
Kuo-Wei Liao, Department of Bioenvironmental Systems Engineering, National Taiwan University, No. 1, Sec. 4, Roosevelt Rd., Taipei 10617, Taiwan.
Email: kliao@ntu.edu.tw

Funding information
Soil and Water Conservation Bureau and Ministry of Science and Technology (MOST) of Taiwan

Abstract

A localized rainfall kinetic energy (E) equation and an erosivity map were developed, and the suitability of the universal soil loss equation (USLE) for assessing the soil erosion of a non-US region was investigated. After accurately measuring and gathering data regarding raindrop size using disdrometers in four northern Taiwan locations, this study investigated the drop size distribution under different conditions by categorizing the rainfall patterns to develop regression equations for estimating the unit volume-specific kinetic energy (KE_{mm}) and the unit time-specific kinetic energy (KE_{time}) of northern Taiwan. Climate zoning, which is not considered in currently used designs, was then implemented along with two-stage cluster analysis to construct a rainfall erosivity (R) distribution map using the kriging model. The binary polynomial regression function of KE_{time}, which had the highest correlation ($R^2 = 0.98$), was suggested to estimate E in northern Taiwan. It was found that the pattern and intensity (I) of rainfall will slightly affect E. The climatic influence on the root mean square of the semivariogram was significant, which suggests that climate zoning can help estimate the rainfall erosivity (R). The outcomes were extended to estimate R in areas without rainfall stations.

KEYWORDS

climate zone, kriging, raindrop size, rainfall erosivity, rainfall kinetic energy

1 | INTRODUCTION

Currently, Taiwan assesses soil erosion using the Universal Soil Loss Equation (USLE), which was developed by Wischmeier and Smith (1978) after gathering soil erosion data and analysing the factors affecting soil erosion across the USA. Among all factors affecting soil erosion, rainfall erosivity (R) and rainfall characteristics are highly correlated (Klik, Kluibenschädl, Strohmeier, Ziadat, & Zucca, 2016), where the former can be used to explicitly quantify the degree of the effects of rainfall and runoff on soil erosion. In an empirical study, Wischmeier and Smith (1958) found that R was positively correlated to the total rainfall kinetic energy (E) and the product of the maximum 30-min rainfall intensity (I_{30}) as shown below:

$$R_j = E_j \times I_{30j} = \sum_{i=1}^{T_i} (e_i P_{ji}) \times I_{30j} \tag{1}$$

where R_j is the R of the jth rain event (MJ mm ha^{-1} h^{-1}); E_j is the E of the jth rain event (MJ ha^{-1}); I_{30j} is the maximum I_{30} (mm hr^{-1}) of the jth rain event; e_i is the unit volume-specific kinetic energy (KE_{mm}) at moment i of the jth rain event (MJ ha^{-1} mm^{-1}); P_{ji} is the rainfall (mm) at moment i of the jth rain event; and T_i is the duration of the jth rain event, in which j represents the number of the rain event and i is moment i of the jth rain event. By summing all the R_j values of the annual total number of rain events (Y), the annual rain erosivity (R_y) is obtained.

$$R_y = \sum_{j=1}^{Y} R_j \tag{2}$$

In Equation (1), e_i is calculated using the rain kinetic energy and the rainfall intensity formulae for Washington D.C., USA, as shown in Equations (3) and (4):

$$e_i = 0.119 + 0.0873 \log_{10} I_i I_i \leq 76\ \mathrm{mm\ hr}^{-1} \tag{3}$$

$$e_i = 0.283\ I_i > 76\ \mathrm{mm\ hr}^{-1} \tag{4}$$

where I_i is the I value at moment i of the jth rain event (mm hr^{-1}). In the revised USLE (RUSLE) published by Renard, Foster, Weesies, McCool, and Yoder (1997), the equation for calculating the unit $\mathrm{KE_{mm}}$ (e_i) is expressed in exponential form, as shown below:

$$e_i = 0.29 \left[1 - 0.72 \exp^{(-0.05 I_i)}\right] \tag{5}$$

Because R is affected by the $\mathrm{KE_{mm}}$ equation and the climate characteristics, to develop an appropriate $\mathrm{KE_{mm}}$ equation for regions outside of the USA, the characteristics of the local climate should be considered. For example, Lee, Lee, and Julien (2018) examined the global and regional scale climatic teleconnections using the rainfall erosivity index variability over South Korea. Rosewell (1986), Angulo-Martínez and Barros (2015), and Lim, Kim, Kim, Park, and Kim (2015) affirmed that the differences in the $\mathrm{KE_{mm}}$ equation for different regions were significant and that the outcomes varied when estimating using the rainfall record of different years (Leek & Olsen, 2006). In addition, $\mathrm{KE_{mm}}$ and raindrop size are correlated. According to Ferrier, Tao, and Simpson (1995), Tokay and Short (1996), and Maki, Keenan, Sasaki, and Nakamura (2001), drop size distribution (DSD), the diameter distribution of the number of raindrops, varied as a result of the intensity and patterns of rainfall. Taiwan, which is located in a subtropical region, experiences different types of rain, including frontal rain, convectional rain and typhoon rain. However, these climatic features were not considered in the $\mathrm{KE_{mm}}$ equations constructed in past studies and were investigated in the current study.

Using the ground-based flour pellet method proposed by Laws and Parsons (1943), Wischmeier and Smith (1958) measured raindrop size and developed the USLE. Because their method could not be used to observe raindrop size at all times and there was still room for accuracy improvements, Rosewell (1986), Angulo-Martínez and Barros (2015), and Lim et al. (2015) collected raindrop size data using a disdrometer to enhance observation accuracy. In addition, as both the RUSLE and the USLE can be used to calculate $\mathrm{KE_{mm}}$ per unit volume, Salles, Poesen, and Sempere-Torres (2002) and Angulo-Martínez and Barros (2015) replaced $\mathrm{KE_{mm}}$ per unit volume with $\mathrm{KE_{mm}}$ per unit time ($\mathrm{KE_{time}}$) to improve the accuracy of the estimation of E.

The calculation of R requires historical records from rainfall observation stations. Currently, interpolation or inverse distance weighting is used to calculate the R of areas without rainfall stations in Taiwan. Biases may occur when estimating R with the data of nearby areas without considering the characteristics of spatial distribution. For example, despite the proximate straight line distance between two locations, if one location is on the windward side while the other is on the leeward side, R can vary significantly. Thus, it is important to recognize the impact of spatial distribution on rainfall erosivity. Similarly, Qin et al. (2016) investigated the influence of spatial distribution and the temporal trends of rainfall erosivity in China.

Currently, Taiwan uses the E equation developed by Wischmeier and Smith (1958) without considering regional climate diversity, and there is still space for accuracy improvements in raindrop size measurement techniques and R distribution. Thus, in this study, four northern Taiwan locations were selected in an attempt to build a localized equation for estimating E with $\mathrm{KE_{mm}}$ or $\mathrm{KE_{time}}$ based on accurate raindrop size measurements and different rainfall patterns. Then, by calculating the R values of areas with rainfall stations using the proposed equation with consideration of the characteristics of spatial distribution, this study established an R distribution map of northern Taiwan to be used as a reference when estimating R in areas without rainfall stations.

2 | DATA AND METHODOLOGY

2.1 | Data

The study area is the northern part of Taiwan with the GPS coordinates of 24°55′53′′N and 121°1′26′′E, including Yilan County, Taipei City, New Taipei City, Keelung City, Taoyuan City and Hsinchu County. The selected area is 7,395 square kilometers, accounting for 20% of Taiwan's area. The northern part of Taiwan has a subtropical monsoon climate, which is affected by the Pacific subtropical high in summer and by the high pressure of the continental cold air mass in winter. The topography includes mountains, hills, terraces, basins and plains. Under the interaction of climatic patterns and topography such as frontal, monsoon and typhoon, the

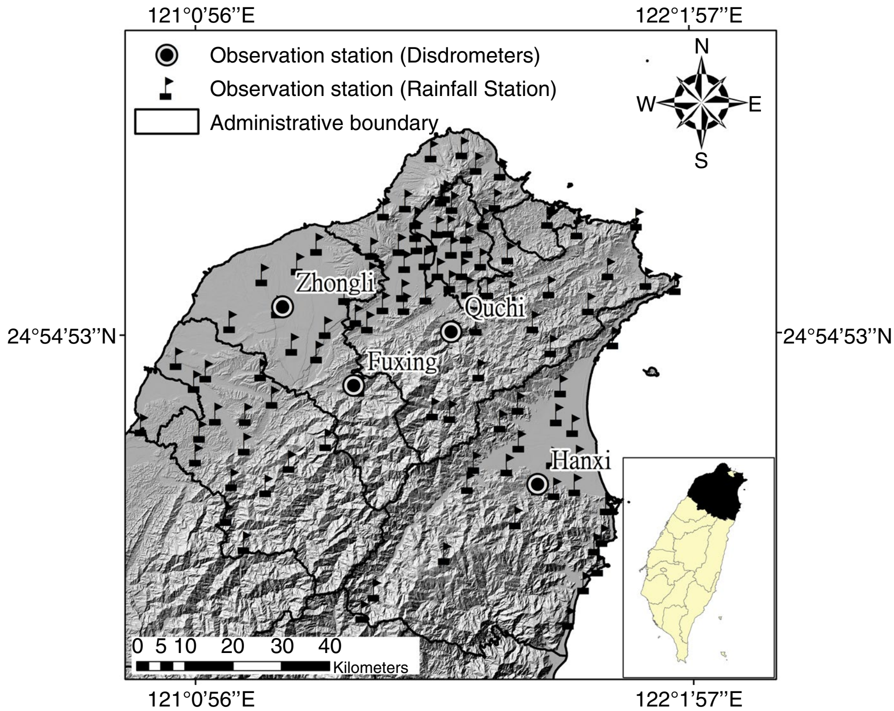

FIGURE 1 Distribution of the disdrometers and rainfall stations in this study

spatial distribution of precipitation is quite complex and varied. The average minimum temperature is 10.1 degrees Celsius in January, and the average maximum temperature is 29.6 degrees Celsius in July. The annual average rainfall is over 2,000 mm in all stations, and the largest is close to 5,000 mm.

This study retrieved data regarding raindrop size, count and rainfall (by minute) between September 2013 and July 2016 from four observation stations with disdrometers in northern Taiwan (Central Station, Feicui Station, Xiayun Station and Hanxi Station). These disdrometers were installed in Zhongli, Fuxing, Quchi and Hanxi. The rainfall data for calculating *R* were retrieved from 153 rainfall stations (between January 2005 and December 2014) distributed as shown in Figure 1. According to Wischmeier and Smith (1978), effective rain events refer to rainfall that is greater than 12.7 mm and only if there are no other rainfall events 6 h apart from the rainfall event in question. Additionally, they refer to rainfall that is less than 12.7 mm but reaches 6.35 mm in 15 min. Based on the effective duration of each rain event, this study considered raindrop size and rainfall every 10 min as unit samples for the estimation of *E*.

2.2 | Methodology

2.2.1 | Judgment of rainfall patterns

Raindrop size varies as the rainfall pattern varies, and this may affect subsequent *E* estimations. After eliminating ineffective rain events in the historical data of individual rainfall stations, this study divided rainfall patterns into frontal rain, stationary frontal rain, typhoon rain and convectional rain according to the yearly climatic characteristics of northern Taiwan. This study also gathered climographs, such as satellite cloud images, radar images and surface weather charts of the period from which raindrop size data were obtained. After contrasting the occurrence of cold fronts, stationary fronts and typhoons with the effective rain events each year, determined from the climographs, this study obtained the rainfall patterns of individual rain events and considered rain events unassociated with cold fronts, stationary fronts or typhoons as convectional rain.

2.2.2 | Rain kinetic energy

This study assumed that all raindrops in the collected raindrop size data are spherical pellets and that the kinetic energy of each raindrop is the mass converted from the drop volume ($V =$ multiplied by the raindrop terminal speed, as shown in Equation (6):

$$E = \mathrm{m}\mathrm{v}^2 \times 2^{-1} \tag{6}$$

where E is the rain kinetic energy (J), m is the raindrop mass (g), and vs the raindrop terminal velocity (cm s^{-1}). The raindrop terminal velocity was calculated based on the equation proposed by Gunn and Kinzer (1949) (same as the USLE), as shown in Equation (7):

$$v^2 = \frac{4}{3}\mathrm{gd}(\rho_s - \rho)\rho^{-1}c^{-1} \tag{7}$$

where g is the gravitational acceleration (980 cm s^{-2}), d is the raindrop diameter (cm), ρ is the fluid density around raindrops (g cm^{-3}), ρ_s is water density, and c is the drag coefficient. Because disdrometers can measure the number of raindrops within a specific period, the total E of a period can be obtained by adding up the kinetic energy of all the raindrops of that period. E is divided into two types: unit volume-specific kinetic energy (KE_{mm}) and unit time-specific kinetic energy (KE_{time}). KE_{mm} is obtained by dividing the total E of a specific period (or a specific rain event) by the total rainfall of that specific period (or specific rain event). While KE_{mm} has units of energy per unit area and per unit rain depth, it is used in both the USLE and the RUSLE. KE_{time} refers to the E of a specific period. While KE_{time} has units of energy per unit area and per unit time, both Salles et al. (2002) and Angulo-Martínez and Barros (2015) investigated E using it in the related literature.

The relationships between KE_{time} and KE_{mm} are shown in Equations (8)–(10).

$$KE_{time} = KET^{-1} \tag{8}$$

$$KE_{mm} = KEP^{-1} \tag{9}$$

$$KE_{mm} = KE_{time} I^{-1} \tag{10}$$

In the above equations, KE is the total E of an effective rain event, P is the total rainfall (mm) of an effective rain event, T is the total rain duration (D), and I is the rainfall intensity (mm hr^{-1}).

2.2.3 | Estimation of the spatial distribution of annual rain erosivity

Based on the collected data on raindrop sizes and counts and the E equation for northern Taiwan, the annual rain erosivity of each rainfall station was obtained by inputting the rainfall data of 153 rainfall stations into Equations (1) and (2) as the foundation for estimating spatial distribution. In order to estimate the spatial distribution of R, this study first implemented climate zoning based on spatial characteristics and rainfall characteristics. The details of these climate characteristics zoning and spatial characteristics zoning approaches are described as follows.

Climate characteristics zoning

Applying spatial analysis to hydrology aims to provide hydrological information of places without installing disdrometers. Zoning must be implemented before carrying out the analysis to group observation stations with a similar hydrology in the same zone to facilitate spatial analysis using point-based or zone-based data. This study adopted multivariate statistical analysis—two-stage cluster analysis—for climate zoning (Punj & Stewart, 1983). Before performing this cluster analysis, several issues, such as parameter selection, standardization and dimension reduction, were necessary and are now introduced. In consideration of the spatial characteristics, the distribution characteristics of effective rain events and the long-term change characteristics of the effective rain events of the 153 observation stations, this study selected 13 analysis parameters, as shown in Table 1. These parameters were standardized before our analysis to obtain a zero mean and unit variance for each parameter. Dimension reduction with principal components analysis (PCA), is a statistical procedure converting a set of observations of possibly correlated variables into a set of values of linearly uncorrelated variables by means of an orthogonal transformation, was conducted to reduce parameters to an acceptable quantity based on the dependency affecting parameters and to avoid the relevance effect among parameters. When determining the principal components, a rule of thumb was applied as a criterion to select principal components with an eigenvalue above unity and to eliminate those with an eigenvalue below unity (Gorsuch, 1983).

Cluster analysis was implemented in two steps: step 1 was a hierarchical cluster analysis and step 2 was a non-hierarchical cluster analysis. The hierarchical cluster analysis was performed pairwise: one group on the PCA outcomes and another group on the standardized parameters. First, this study performed hierarchical cluster analysis using the Ward method (Ward, 1963) and judged the number of clusters with the condensed coefficient. If the coefficient escalates, merging is inappropriate. Then, this study performed the non-hierarchical analysis using the K-means along with the number of clusters obtained from the hierarchical cluster analysis to obtain more stable clustering results (Punj & Stewart, 1983).

Estimation of spatial distribution

By estimating the annual rain erosivity using the ordinary kriging model on the effective rain events between 2005 and 2014 of all the observation stations in terms of the following three groups: the entire northern Taiwan region, zoning by raw but standardized parameters and zoning via PCA. The effects on the accuracy of the spatial distribution of R for different climatic zoning approaches were then investigated. The experimental pairwise semivariogram of the 153 observation stations was calculated using Equation (11) as described below:

$$\gamma(h) = \frac{\sum_{n=1}^{k} [z(x_i + h) - z(x_i)]^2}{2k} \tag{11}$$

TABLE 1 Parameter selection for climate zoning

Parameter type	Parameter	Unit
Spatial characteristics of observation station	1. Station elevation	m
	2. Station longitude	o
	3. Station latitude	o
Distribution characteristics of effective rain events	4. Annual average of effective rain events	Event
	5. Annual average of rain duration	h
	6. Annual average rain intensity	mm hr^{-1}
	7. Annual I_{30}	mm hr^{-1}
	8. Annual average R (R_{ave_Year})	MJ mm ha^{-1} hr^{-1}
Long-term changes in the characteristics of effective rain events	9. cov of the annual average of effective rain events	%
	10. cov of the annual average of rain duration	%
	11. cov of the annual average of rain intensity	%
	12. cov of the annual average of I_{30}	%
	13. cov of the annual average of R	%

Abbreviation: cov stands for the coefficient of variation.

where $z(x_i)$ is the R of station i; k is the number of matched pairs of x_i and x_j, $h = x_i - x_j$ is the relative distance between x_i and x_j. According to Journel and Huijbregts (1978), there must be over 30 pairs of data for each distance and the interval of each pair must be below the maximum value of the two stations. Six theoretical semivariogram equations (linear, power series, exponential, spherical, circular and Gaussian) were first optimized based on the experimental variogram of all points at all intervals. When calculating the coefficient of each model, multiple initial values were applied to prevent falling into the local optimal solutions.

After constructing all theoretical semivariogram models, the fittest model was determined via cross-examination. First, one observation station ($z(x_1)$) was selected from among all stations. Then, a kriging estimation was conducted on $z(x_1)$ with the other observation stations ($n-1$) to obtain the estimated value of the selected observation station and calculate the estimated error of $z(x_1)$. The aforementioned process was repeated until the values for all observation stations were estimated. Lastly, the difference between the actual value and the estimated value of all the theoretical models was obtained. The one with the lowest root mean square error was selected as the fittest theoretical model for this study. A linear combination of the weighted coefficients of the theoretical semivariogram model and the observation values can be used to estimate unknown points, as shown in Equation (12):

$$\hat{Z}(x_0) = \sum_{i=1}^{n} \lambda_i Z(x_i) \tag{12}$$

where $\hat{Z}(x_0)$ is the kriging estimation at the non-sampled location x_0, $Z(x_i)$ is the value sampled at locationx_i, λ_i is the weight factor of $Z(x_i)$, and n is the number of scattered points in the set. The resolution (2.5 km) of the Advanced Regional Prediction System (ARPS) of the Central Weather Bureau was used as a reference in this study. After zoning northern Taiwan with a 2.5 by 2.5 km grid with its centre as the estimated location, this study constructed the distribution map of the annual average R of northern Taiwan.

3 | ANALYSIS RESULTS

To estimate a suitable erosivity map, several important factors, such as DSD, rain kinetic energy and spatial distribution, were investigated. Detailed results and important observations are provided below.

3.1 | Investigation of drop size distribution

Observing that there were significant differences in the size distribution of raindrops reaching the ground from frontal clouds, Mason and Andrews (1960) investigated the DSD of various types of rain. Chien (2005) investigated raindrop size distribution in different seasons and rain types in Taiwan and indicated that, as rainfall increases, the number of greater raindrops increases and the raindrop size distribution extends to the right. Based on the results of the aforementioned past study, this study attempted to investigate the DSD differences for different rain intensities and rain patterns. To accomplish this task, the study collected the cumulative percentages of raindrop volume every 10 min of effective rain events, as shown in Figures 2 and 3. Each line represents the 10-min DSD of each rain event, the x-axis represents raindrop size, and the y-axis represents the cumulative percentage of volume of a particular raindrop size during that rain event. Figure 2 shows that the cumulative distribution curve of raindrop volume was inclined to the right for rain events with

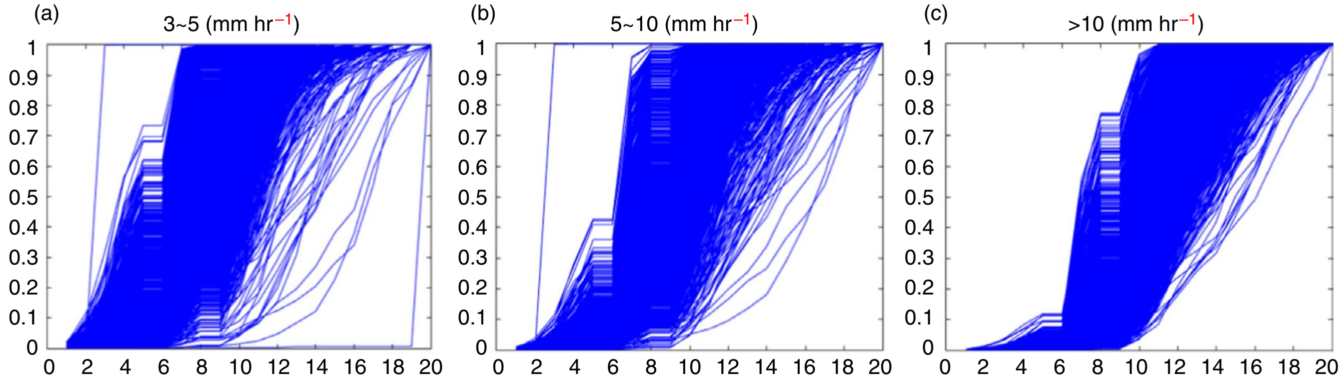

FIGURE 2 Curves of cumulative raindrop volume distribution of rain incidents by rain intensity (*x*-axis is raindrop size in mm, and *y*-axis is the cumulative volume percentage)

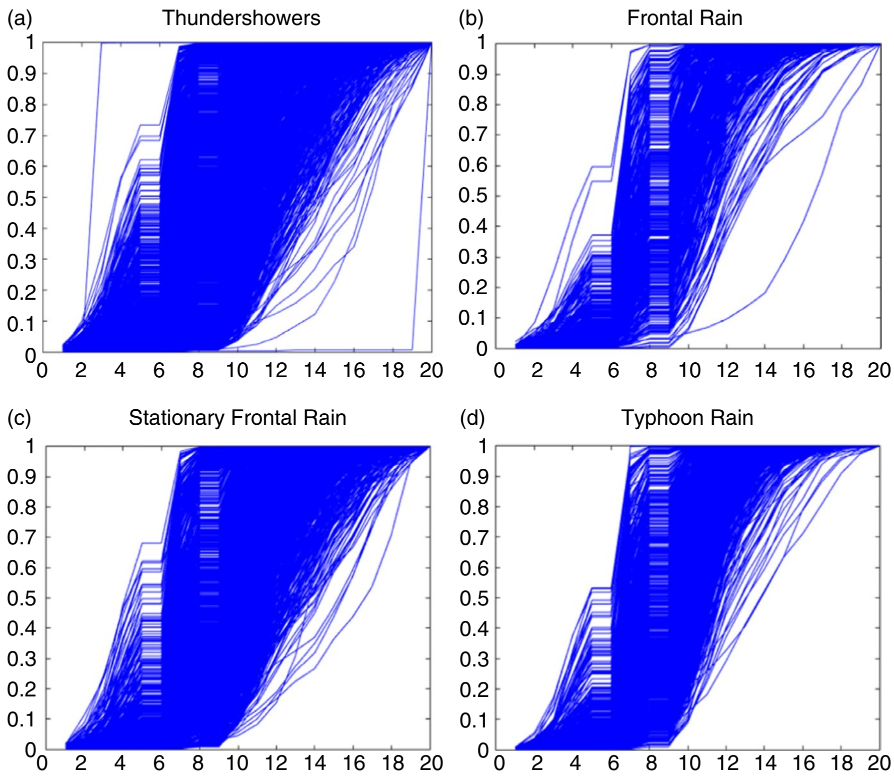

FIGURE 3 Curves of cumulative raindrop volume distribution of rain incidents by rain pattern (*x*-axis is raindrop size in mm, and *y*-axis is the cumulative volume percentage)

greater rain intensities. However, no specific inclination was observed for rain events of lower rain intensity. Therefore, when categorizing by rain intensity, a better result was obtained for rain events with greater rain intensities. However, no significant DSD difference was observed for rain events of lower rain intensities. Figure 3 shows that no significant DSD difference was observed when categorizing by rain pattern, that is, rain patterns were unable to effectively differentiate raindrop size. To further investigate the effect of rain intensity and pattern, four rain patterns and three rain intensities were used to classify 12 types of rain events. Results are similar to a previous study (Mason & Andrews, 1960): neither rain pattern nor rain intensity could affect differential raindrop sizes.

3.2 | Construction of the equation for estimating rain kinetic energy

After obtaining the rainfall data, this study classified the effective rain events and transformed them into data consisting of 10-min unit effective rain events to calculate KE_{mm} and KE_{time} in order to construct the E estimation equation based on E and I.

3.2.1 | Volume-specific kinetic energy-based formula

Figure 4 shows the results of our regression analysis of the KE_{mm} and I of all samples disregarding rain patterns and rain intensity, which indicate that the R^2 difference of the prediction

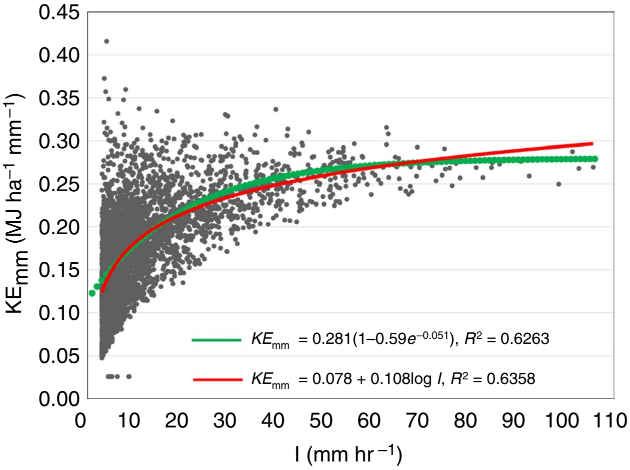

FIGURE 4 Regression analysis of rain intensity (I) with KE_{mm}

equation using either the logarithm or the exponent was insignificant (0.626 vs. 0.636). In addition, among many other functions, the R^2 of the logarithm or the exponent was highest, suggesting that both functions were better choices to describe the correlation between KE_{mm} and I. This observation is similar to the suggestion implied by the USLE and the RUSLE, for which the logarithmic or exponential functions were selected to describe the correlation between KE_{mm} and I. The USLE/RUSLE and the proposed equations were provided in Equation (13). A slight difference was observed, suggesting that there is a need to use the local rainfall data of Taiwan.

$$\begin{cases} \text{USLE:} \quad KE_{mm} = 0.119 + 0.0873 \log I \\ \text{Current:} \quad KE_{mm} = 0.078 + 0.108 \log I \\ \text{RUSLE:} KE_{mm} = 0.29(1 - 0.72 \exp(-0.05I)) \\ \text{Current:} KE_{mm} = 0.28(1 - 0.59 \exp(-0.05I)) \end{cases} \tag{13}$$

Table 2 shows the results of our regression analysis using the linear, logarithmic (USLE) and exponential (RUSLE) models after categorizing the samples into 12 groups by rain pattern and by rain intensity. Figure 5 shows the results of our regression analysis using the logarithmic function. Overall, both the graphs of the logarithmic function and the exponential function can better describe the trend of the data changes among the different groups. However, the results of our graphs and regression analyses show that neither function can effectively enhance equation effectiveness after categorizing samples by rain pattern and by rain intensity. These results were similar to those for DSD. In real rain events, no effective control factor has been found for differential DSD. In terms of our analysis results using the proposed KE_{mm} equation, which was constructed based on the E estimation equation for uncategorized data, results similar to those of past studies (Salles et al., 2002) were obtained.

3.2.2 | Time-specific kinetic energy-based formula

Figure 6 shows our regression analysis of rain intensity (I) with KE_{time} for all samples without categorization by rain pattern and rain intensity. As shown, four types of functions were used for defining the relationship between the two, and their R^2 values were all greater than 0.90, that indicating promising results were obtained for each trial function. Except for the power series function with a lower value, the R^2 of all other types of functions was above 0.97, and the best two results were obtained using the logarithmic and polynomial functions as described in Equation (14).

$$\begin{cases} KE_{time} = \quad 0.0157I + 0.0159I \log I \\ KE_{time} = 0.000088I^2 + 0.039I - 0.073 \end{cases} \tag{14}$$

Similarly, regression analysis of samples after categorizing them into 12 groups by rain pattern and by rain intensity

TABLE 2 R^2 value of KE_{mm} by rain pattern and by rain intensity

	Thundershowers			**Frontal rain**		
	Linear	**Exponent**	**Logarithm**	**Linear**	**Exponent**	**Logarithm**
I = 3–5 mm hr^{-1}	0.19	0.19	0.19	0.22	0.22	0.22
I = 5–10 mm hr^{-1}	0.23	0.24	0.23	0.28	0.28	0.28
I = > 10 mm hr^{-1}	0.50	0.57	0.58	0.57	0.60	0.60
	Stationary frontal rain			**Typhoon rain**		
	Linear	**Exponent**	**Logarithm**	**Linear**	**Exponent**	**Logarithm**
I = 3–5 mm hr^{-1}	0.16	0.17	0.16	0.002	0.01	0.003
I = 5–10 mm hr^{-1}	0.32	0.32	0.32	0.18	0.18	0.18
I = >10 mm hr^{-1}	0.57	0.60	0.61	0.55	0.54	0.53

Note: Linear: e_{mm} = A*I + B; Logarithm: e_{mm} = A*logI + B; Exponent: $e_{mm} = A*e^{-0.05I} + B$.

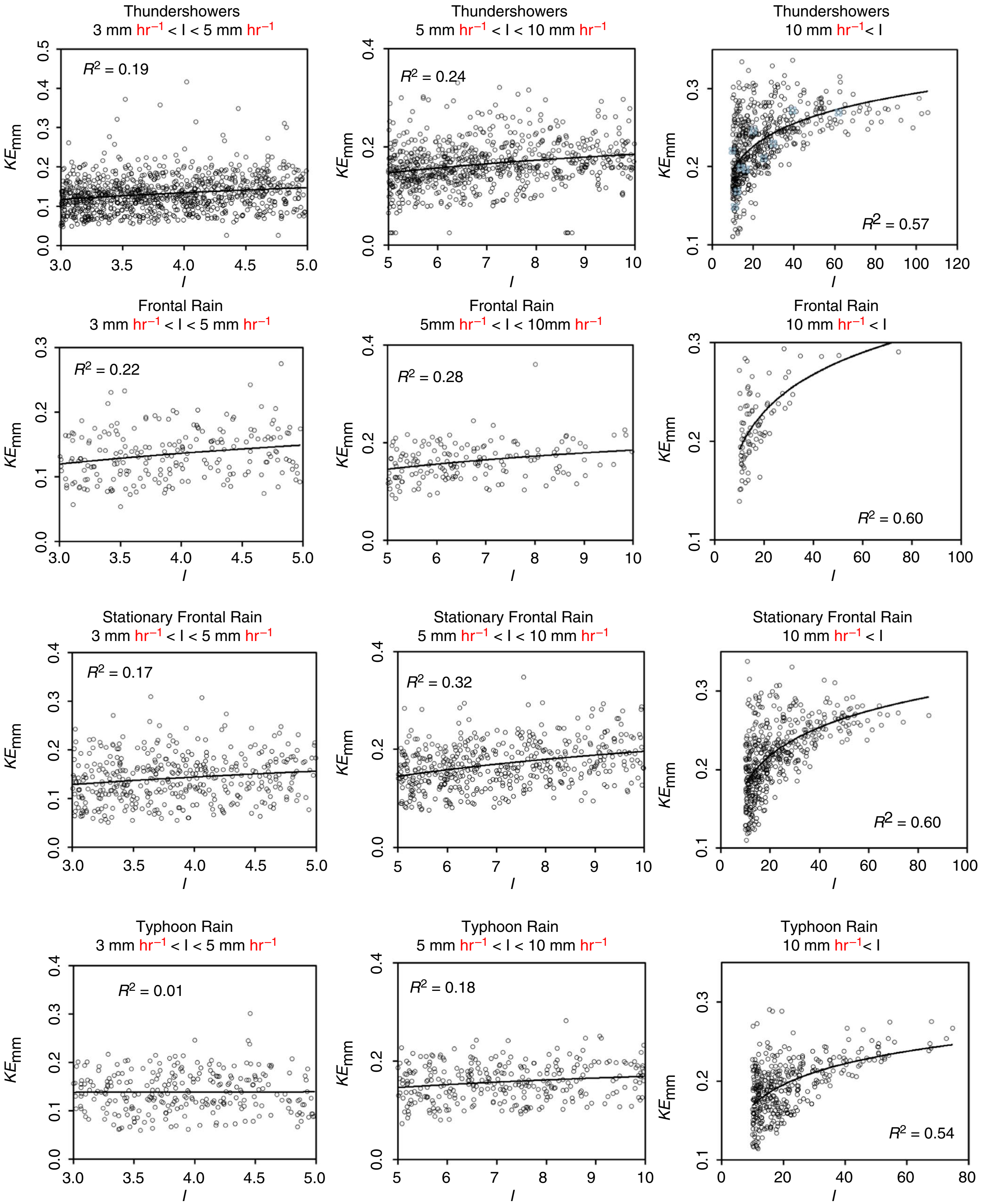

FIGURE 5 Regression analysis of rain intensity (I) with KE_{mm} (categorization by rain pattern and rain intensity)

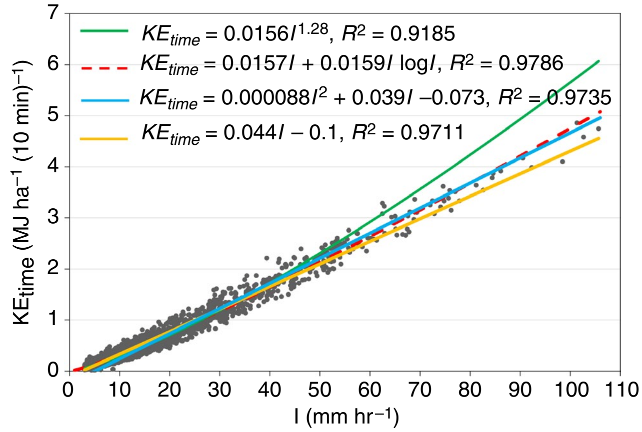

FIGURE 6 Regression analysis of rain intensity (I) with KE_{time}

TABLE 3 Results of principal components analysis

Parameter	Principal component 1	2	3	4	5
Elevation			0.779		
Longitude	0.665				
Latitude			−0.806		
Effective rain events	0.902				
Rain duration	0.679				
Rain intensity		0.848			
I_{30}		0.930			
Rain erosivity	0.730				
Effective rain event cov	−0.700				
Rain duration cov					0.923
Rain intensity cov				0.919	
I_{30} cov		−0.638			
Rain erosivity cov			0.685		

was conducted with respect to KE_{time}. These results were similar to those of our regression analysis without sample categorization except when the rain intensity was above 10 mm hr^{-1}. However, they were less accurate than the results of our regression analysis without sample categorization when rain intensity was below 10 mm hr^{-1}. Both cases yielded similar results to those of our regression analysis using KE_{time}. Because the results of our regression analysis without sample categorization were highly correlated, KE_{time} was sufficient to estimate E.

Based on these analysis results, it was found that KE_{time}, investigated by Salles et al. (2002) and Angulo-Martínez and Barros (2015), was a better indicator of rain intensity (I). In addition, there was no significant influence when the four proposed rain patterns and three rain intensities were considered.

3.3 | Estimation of the spatial distribution of rain erosivity

3.3.1 | Zoning by climatic characteristics

Table 3 shows the PCA results. As shown in the table, five principal components (PCs) were extracted. PC1 was the rain erosion characteristic factor comprising effective rain events, rain erosivity, rain duration and the coefficient of variation (CV) of effective rain events; PC2 was the rain intensity factor comprising rain intensity, maximum 30-min rainfall intensity (I_{30}) and the CV of I_{30}; PC3 was the observation station location factor comprising elevation and latitude; PC4 was the long-term rain intensity variance comprising the CV of rain intensity; and PC5 was the long-term rain duration variance comprising the CV of rain duration. Table 4 shows the results of the analysis of condensed clusters of each group in our hierarchical analysis. There were six clusters after PCA and five clusters of raw parameters. Because there were fewer observation stations in the cluster set, a cluster of few observation stations might affect the representativeness of the results of subsequent spatial distribution estimations. For this reason, a latitude map was appended to the results in Table 4 to perform climate zoning. Based on the above approach, northern Taiwan was divided into two zones (M1 and M2) when using PCA and three zones (O1, O2 and O3)

TABLE 4 Results of hierarchical cluster analysis of different groups

Parameter	PCA			Raw parameters		
Condensation process	Clusters	Coefficient	Coefficient difference	Clusters	Coefficient	Coefficient difference
	6	34.961	1.761	6	12.036	0.967
	5	36.138	1.177	5	16.585	4.549
	4	40.896	4.758	4	18.368	1.783
	3	42.315	1.419	3	21.334	2.966
	2	63.300	20.985	2	22.764	1.430
	1	86.886	23.586	1	40.931	18.167
Clusters	5			6		

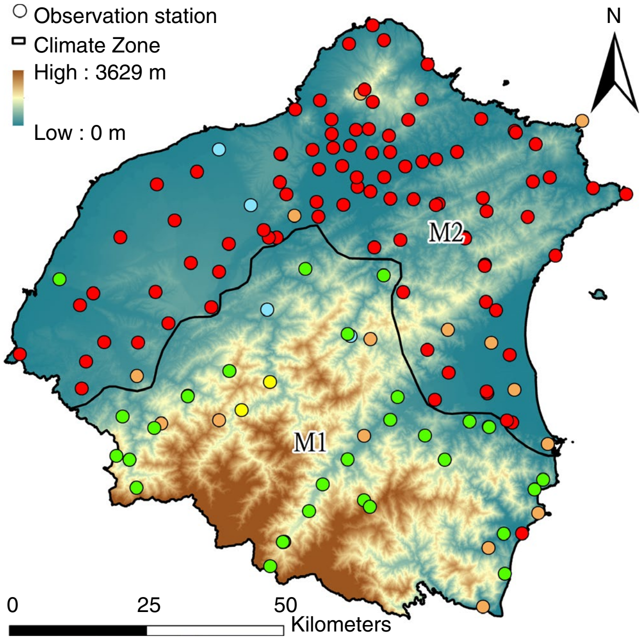

FIGURE 7 Results of climate zoning with PCA

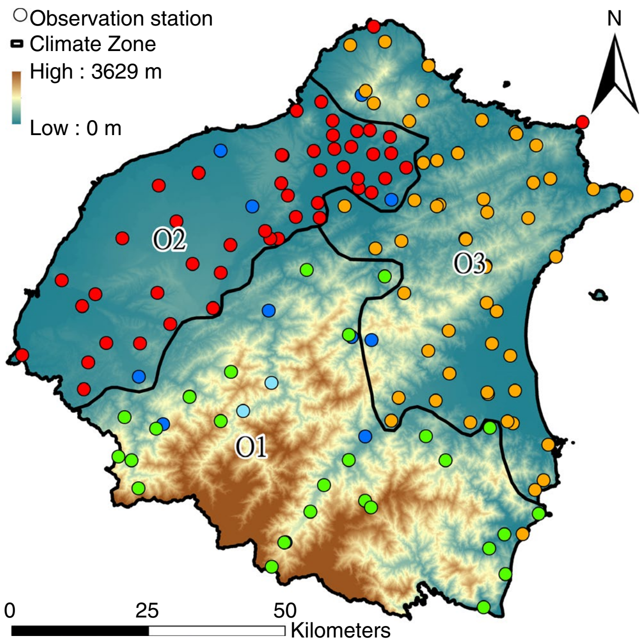

FIGURE 8 Results of climate zoning with raw parameters

when using the raw parameters, as shown in Figures 7 and 8, respectively.

3.3.2 | Estimation of spatial distribution

Table 5 shows the R-testing results over the years using the semivariogram model before zoning and after zoning with the raw parameters and zoning with PCA. Except for the results of 2013, better results in terms of the root mean squared error (RMSE) were obtained using PCA and the raw parameters, suggesting that the RMSE after climate zoning was smaller than that before climate zoning. This means that the climate zoning approach proposed in this study can help estimate the spatial distribution of rain erosivity. Please note that the smallest RMSE in the semivariogram model of each year was used to estimate the rain erosivity of the unknown grids in each year. Details of the RMSEs in the semivariogram model over the years are not provided here. Figure 9 shows the results of our rain erosivity estimations over the years.

TABLE 5 Rain erosivity RMSE in the semivariogram model over the years

Year	Before zoning	PCA	Raw parameters
2005	1.130×10^4	1.147×10^4	9.896×10^3
2006	5.529×10^3	5.167×10^3	4.481×10^3
2007	9.438×10^3	9.035×10^3	8.558×10^3
2008	1.261×10^4	1.105×10^4	1.072×10^4
2009	7.774×10^3	7.505×10^3	7.568×10^3
2010	6.095×10^3	6.143×10^3	5.862×10^3
2011	6.720×10^3	6.714×10^3	6.495×10^3
2012	6.562×10^3	6.294×10^3	6.548×10^3
2013	5.177×10^3	5.251×10^3	5.259×10^3
2014	4.094×10^3	3.951×10^3	4.186×10^3

To further understand the difference between the proposed rain erosivity and the current rain erosivity, which is provided in the soil and water conservation manual of Taiwan (2018), the ratio of the proposed and the current rain erosivities was calculated, as shown in Figure 10. It can be seen that the ratio ranged from 0.72 to 3.23. The rain erosivity in the Taipingshan area increased the most. If the R value in the current soil and water conservation manual is used for engineering designs, the risks implied by each region are different. The risk involved with sedimentation tanks is considered using a safety factor of 1.5. As shown in Figure 10, there were many regions where the *R* value growth rate was more than 1.5 times the safety factor. It can be seen that the annual rainfall erosion data in northern Taiwan need to be revised and updated.

4 | CONCLUSIONS

After collecting raindrop size data in northern Taiwan (Central Station, Fecui Station, Hayun Station and Hanxi Station) using automatic disdrometers and categorizing by rain pattern, this study investigated the DSD characteristics under different conditions and tested the regression effects of KE_{mm} and KE_{time} with rainfall intensity I to develop a localized rain

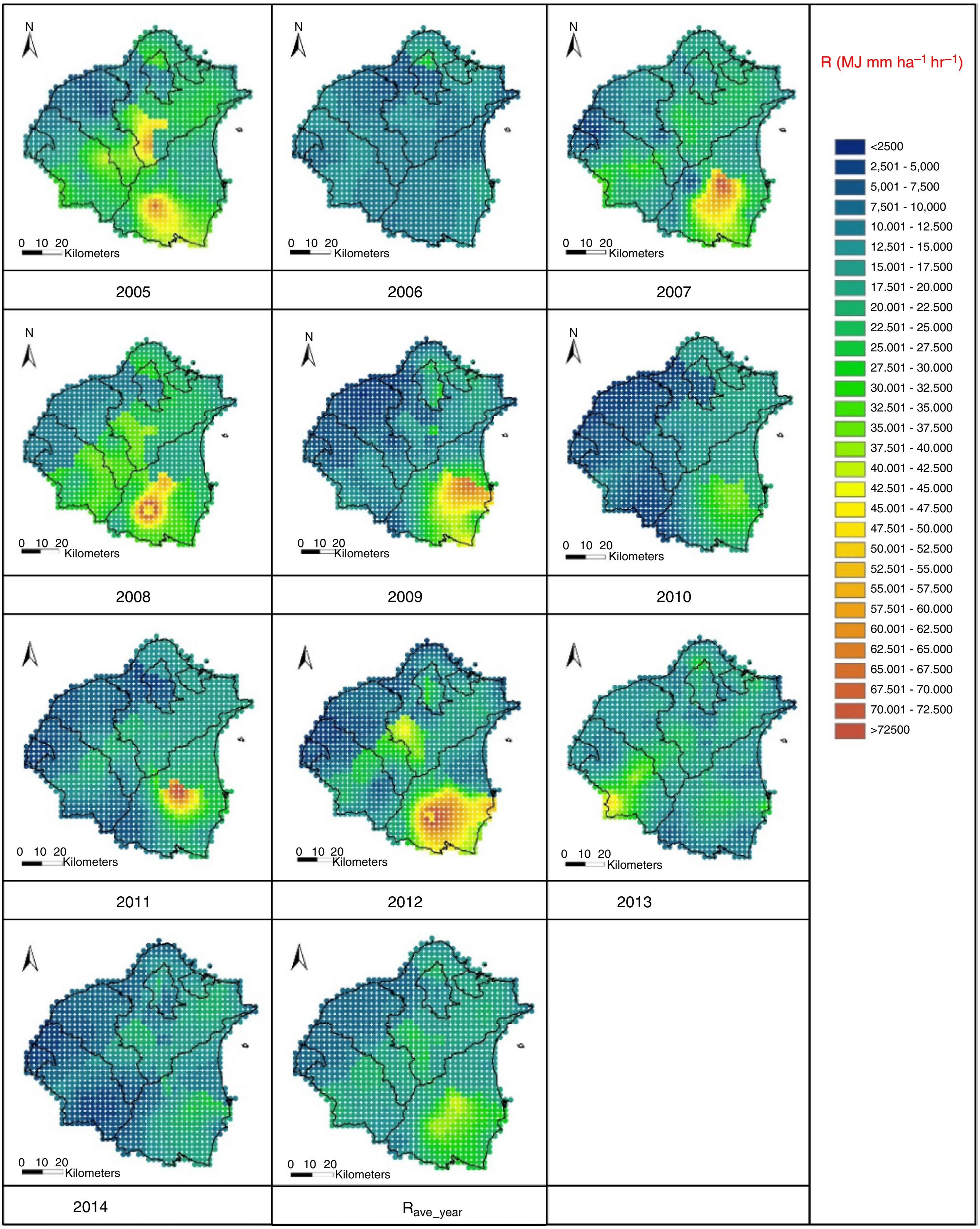

FIGURE 9 Results of annual rain erosivity estimation in northern Taiwan over the years

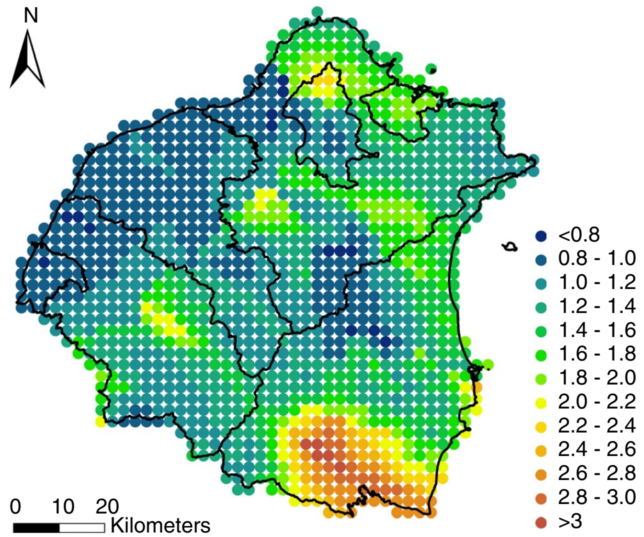

FIGURE 10 Ratios of the proposed to the current R values

kinetic energy equation for northern Taiwan. On the basis of the established rain kinetic energy equation, this study further constructed an R distribution map. Please note that the aforementioned methodology, established in this study, is readily applied to other regions of Taiwan. For example, the central and eastern portions of Taiwan are currently understudied using similar approach. Some valuable outcomes and conclusions of this study are described as follows:

1. After testing the regression effect of KE_{mm} with rainfall intensity I, the results of this study were similar to those of past studies. However, slight differences were found in the equation coefficients developed for different regions (e.g. the USA and Taiwan). Therefore, in rain kinetic energy estimations, using rainfall data from Taiwan can help to better estimate rain kinetic energy.
2. After testing the regression effect of KE_{time} with rain intensity I, promising results were obtained with different types of functions as indicated in Figure 6 ($R^2 \geq 0.90$), and the prediction results of the binary polynomial function were one of the best ($R^2 = 0.97$). Therefore, both the logarithmic and polynomial functions, as described in Equation (14), are suggested for estimating the rain kinetic energy in northern Taiwan.
3. The effect of rain pattern and rain intensity on the regression results was insignificant (KE_{time} vs. I), and the results without categorization were sufficient to estimate rain kinetic energy.
4. When estimating the spatial distribution with R, the semivariogram RMSE after climate zoning was smaller than that before climate zoning. This suggests that climate zoning can help estimate the spatial distribution of rain erosivity, and the results can serve as a reference for estimating the R value of areas without rainfall stations.

ACKNOWLEDGEMENTS

The authors would like to thank the Soil and Water Conservation Bureau and Ministry of Science and Technology (MOST) of Taiwan for their support that enabled the smooth completion of this study.

ORCID

Kuo-Wei Liao https://orcid.org/0000-0001-5274-291X

REFERENCES

Angulo-Martínez, M., & Barros, A. P. (2015). Measurement uncertainty in rainfall kinetic energy and intensity relationships for soil erosion studies: An evaluation using PARSIVEL disdrometers in Southern Appalachian Mountains. *Geomorphology*, *228*, 28–40. https://doi.org/10.1016/j.geomorph.2014.07.036

Chien, C. L. (2005). *The characteristics of drop size distribution in different seasons and rain-types in Taiwan*. Master Thesis of National Central University, Taiwan.

Ferrier, B. S., Tao, W. K., & Simpson, J. (1995). A double-moment multiple-phase four-class bulk ice scheme. part II: Simulations of convective storms in different large- scale environments and comparisons with other bulk parameterizations. *Journal of the Atmospheric Sciences*, *52*, 1001–1033. https://doi.org/10.1175/1520-0469(1995)052<1001:ADMMPF>2.0.CO;2

Gorsuch, R. L. (1983). *Factor analysis*. Hillsdale, NJ: Lawrence Erlbaum Associates.

Gunn, R., & Kinzer, G. D. (1949). The terminal velocity of fall for droplets in stagnant air. *Journal of Meteorology*, *6*, 243–248. https://doi.org/10.1175/1520-0469(1949) 006<0243:TTVOFF>2.0.CO;2

Journel, A. G., & Huijbregts, C. H. (1978). *Mining geostatistics*. London, UK: Academic Press.

Klik, A., Kluibenschädl, F., Strohmeier, S., Ziadat, F., & Zucca, C. (2016). Assessment of gully erosion using conventional field measurements: A case study from northern Ethiopia. *Journal of Soil and Water Conservation*, *71*(6), 134A–139A. https://doi.org/10.2489/jswc.71.6.134A

Laws, J. O., & Parsons, D. A. (1943). The relation of raindrop-size to intensity. *Transactions American Geophysical Union*, *24*, 452–460. https://doi.org/10.1029/TR024i002p00452

Lee, J. H., Lee, J. H., & Julien, P. Y. (2018). Global climate teleconnection with rainfall erosivity in South Korea. *Catena*, *167*, 28–43. https://doi.org/10.1016/j.catena.2018.03.008

Leek, R., & Olsen, P. (2006). Modelling climatic erosivity as a factor for soil erosion in Denmark: Changes and temporal trends. *Soil Use and Management*, *16*(1), 61–65. https://doi.org/10.1111/j.1475-2743.2000.tb00175.x

Lim, Y. S., Kim, J. K., Kim, J. W., Park, B. I., & Kim, M. S. (2015). Analysis of the relationship between the kinetic energy and intensity of rainfall in Daejeon, Korea. *Quaternary International*, *384*, 107–117. https://doi.org/10.1016/j.quaint.2015.03.021

Maki, M., Keenan, T. D., Sasaki, Y., & Nakamura, K. (2001). Characteristics of the raindrop size distribution in tropical continental squall lines observed in Darwin, Australia. *Journal of Applied Meteorology*, *40*, 1393–1412. https://doi.org/10.1175/1520-0450(2001) 040<1393:COTRSD>2.0.CO;2

Mason, B. J., & Andrews, J. B. (1960). Drop-size distributions from various types of rain. *Quarterly Journal of the Royal Meteorological Society*, *86*(369), 346–353. https://doi.org/10.1002/qj.49708636906

Punj, G., & Stewart, D. W. (1983). Cluster analysis in marketing research: Review and suggestions for application. *Journal of Marketing Research*, *20*(2), 134–148. https://doi.org/10.2307/3151680

Qin, W., Guo, Q., Zuo, C., Shan, Z., Ma, L., & Sun, G. (2016). Spatial distribution and temporal trends of rainfall erosivity in mainland China for 1951–2010. *Catena*, *147*, 177–186. https://doi.org/10.1016/j.catena.2016.07.006

Renard, K. G., Foster, G. R., Weesies, G. A., McCool, D. K., & Yoder, D. C. (1997). *Predicting soil erosion by water – A guide to conservation planning with the revised Universal Soil Loss Equation (RUSLE)*. Agricultural Handbook, 703, Washington, DC: US Government Printing Office.

Rosewell, C. J. (1986). Rainfall kinetic energy in eastern Australia. *Journal of Climatology and Applied Meteorology*, *25*, 1695–1701. https://doi.org/10.1175/1520-0450(1986) 025<1695:RKEIEA>2.0.CO;2

Salles, C., Poesen, J., & Sempere-Torres, D. (2002). Kinetic energy of rain and its functional relationship with intensity. *Journal of Hydrology*, *257*(1–4), 256–270. https://doi.org/10.1016/S0022-1694(01)00555-8

Soil and Water Conservation Bureau, Council of Agriculture, Execute Yuan of Taiwan (2018). *Soil and water conservation manual*. Taipei, Taiwan: Soil and Water Conservation Bureau, Council of Agriculture, Execute Yuan of Taiwan.

Tokay, A., & Short, D. A. (1996). Evidence from topical raindrop spectra of the origin of rain from stratiform versus convection clouds. *Journal of Applied Meteorology*, *35*, 355–371.

Ward, J. H. Jr (1963). Hierarchical grouping to optimize an objective function. *Journal of the American Statistical Association*, *58*(301), 236–244. https://doi.org/10.1175/1520-0450(1996)035<0355:EFTRSO>2.0.CO;2

Wischmeier, W. H., & Smith, D. D. (1958). Rainfall energy and its relationship to soil loss. *Geophysical Union*, *39*(2), 285–291. https://doi.org/10.1029/TR039i002p00285

Wischmeier, W. H., & Smith, D. D. (1978). *Predicting rainfall erosion losses – a guide to conservation planning*. U.S. Department of Agriculture, Agriculture Handbook, 537, Washington, DC: US Government Printing Office.

How to cite this article: Liao K-W, Guo J-J, Fan J-C, Lee C-C, Huang CL. Evaluation of rainfall kinetic energy and erosivity in northern Taiwan using kriging with climate characteristics. *Soil Use Manage*. 2019;00:1–13. https://doi.org/10.1111/sum.12519